Journal of University of Babylon for Engineering Sciences, Vol. (27), No. (4): 2019.

New Model for Passive Vibration Control of Cantilever Beams Using Two Patches of Fluidic Flexible Matrix Composite Tubes

Shireen O. Mohammad

Mechanical and Mechatronics, Engineering collage, Salahaddin University-Erbil, Iraq.

shireen.muhammad@su.edu.krd

Nazhad A. Hussain

Mechanical and Mechatronics, Engineering collage, Salahaddin University-Erbil, Iraq.

nazhad.hussein@su.edu.krd

Submission date:- 21/7/2019	Acceptance date:- 4/9/2019	Publication date:- 11/10/2019

Abstract

Flexible Matrix Composite (F^2MC) tubes are emerging technologies, which can provide lightweight, compact vibration control when attached to a vibrating structure. This work presents a new model for solving a problem of vibrations in cantilever beams with attaching F^2MC tubes as patches that provide passive vibration control. Mathematical model of the compound system of patches of F^2MC tubes integrated on the beam was derived. The governing equations depend on Euler-Bernoulli beam theory and Lekhnitskii's theory of elasticity. This study examined new model's performance for damping with variation in tube size; bonding position of the patches on the beam in two different cases: on the beam through changing the distance between two them; one patch above and the other under the beam. Analytical results demonstrate that the proper tuning the size of tubes as a function of inner layer radius; and integration points are basic parameters for passive vibration control. They achieve reductions in response amplitude at the first vertical bending mode effectively.

Keywords:- Passive vibration controller, Fluidic flexible matrix composite tubes, Mathematical model, Damping, Frequency response function.

Nomenclature

d= the distance between the neutral axis of the tubes and the centerline of the beam.

ε_r^i = Raidial strain of the inner layer.

ε_r^o =Raidial strain of the outer layer.

ε_z^i = Axial strain of the inner layer.

ε_z^m= Axial strain of the middle layer

ε_θ^i =Tangential strain of the inner layer.

ε_θ^m= Tangential strain of the middle layer.

ε_θ^o= Axial strain of the outer layer.

ε_r^m= Radial strain of the middle layer

σ_r^i= Radial stress of the inner layer.

σ_r^o= Radial stress of the outer layer.

σ_z^o= Axial stress of the outer layer.

σ_θ^i= Tangential stress of the inner layer.

σ_θ^o= Tangential stress of the outer layer.

F_{t1}, F_{t2}= Extension force on the F^2MC patches

G_p=Transfer function of F^2MC tubes

L=Beam length

L_{FMC} =Length of F^2MC tube

M1, M2= The moments that formulated on the patches.

P_1= inner layer's surface pressure

P_2= Middle layer's surface pressure

P_3=Outer layer's surface pressure

P_o= Internal surface pressure (fluid pressure)

T=axial Force on the F^2MC tube

T_1, T_2, T_3= Individual forces on the layers of F^2MC tubes.

y(x,t) =beam displacement

σ_z^i=axial stress of the inner layer.

Vi=initial volume of the F^2MC tubes

1. Introduction

In advanced applications, the design of some structures, such as those in spacecraft, jet fighters and automobiles which require lightweight strength and have highly structural damping properties, are faced with great difficulty due to the fact that the decreased weight results in low rigidity and reacts with vibration characteristics. Vibration must be effectively controlled, otherwise it could be uncomfortable for human beings, increase fatigue, cause instability and could result in damage to the entire system [1]. Tuned Vibration Absorbers (TVAs) are important engineering tools for vibration suppression. They can take the form of passive, semi-active or active vibration control devices[2].TVAs without damping that are composed of springs and mass elements can overcome a specific amount of disturbance[3].

In advanced technologies, various vibration control technics have been used in modern vibration control design for smart structures. Researcher [2], has been used Tuned Mass Dampers (TMDs) for controlling vibrations over a small frequency ranges. Damping treatment of cantilever beams had been studied by using electro-magnetic compressional damping treatment [4]. Another study[5], investigated a theoretical control technique using piezo ceramic sensors and actuators along with Multi Input and Multi Output Linear Quadratic Gaussian (MIMO LQG) controller. Experimental validations achieved that MIMO LOG controller was efficient for the suppression of vibrations on cylindrical shells by 13dB.

Fluidic Flexible Matrix Composite (F^2MC) tubes were made from a new type of lightweight and adaptive smart materials. They are economic, use readily-available materials. These tubes have great tailorability, high fluid pumping efficiency, and variable stiffness properties, with ease of integration on structures. They first discovered as variable volume tubes with large modulus ratios [6, 7]. The main parameters of a F^2MC tube is the anisotropic composite laminated layer with fibres oriented at $\pm\alpha$ with a longitudinal axis with their length. The places that the tubes are bonded on the structures, and valve which controls a fluid flow also have an effective role for tailoring the tube's behaviour. Philen, et al. [6] showed that by tailoring the fibre orientation and fluid bulk modulus, these tubes can work as flexible materials when the valve is open and as very stiff when the valve is closed. Ying Shan, et al. [8] investigated F^2MC tubes for autonomous structural tailoring. A model of single F^2MC tube has been analyse and validated experimentally. their results showed the maximum modulus ratio can be obtained by using a composite laminate fibre angle ($\alpha \approx 20°$), or decreasing the tube thickness, or increasing the fluid bulk modulus. Vashisth, et al. [9] evaluated a three-layered F^2MC tube which was two millimetres in diameter, consisted of polyurethane reinforced with braided stainless-steel wire in the middle layer, surrounded by polyurethane layers. Blocked force, free strain and axial modulus of elasticity has been examined. Lotfi-Gaskarimahalle, et al. [10] developed a 3D model for F^2MC tubes and a lumped fluid mass as a novel TVA. It provided a close form of isolation frequency depending on the orifice flow coefficient and the orifice size. The results indicated that F^2MC TVA is robust in terms of mass variations, and increasing damping ratios are achievable with increase in the orifice viscous damping. Philen [11] showed the F^2MC tubes performance for base isolation mounts. Recently, through series investigations these tubes performance as vibration absorbers has been studied. They has been connected with two fluidic circuits, the first damped out vibrations over 20dB by using orifice; the latter circuit used an inertia track and an accumulator, replaced the first mode resonance peak with a valley, reduced the resonant response by 27dB, [12]. This was followed by a design of multi-layered F^2MC patch fixed on a cantilever beam with a distance (x_1) far from the fixed end, [13]. Water was used as working medium. Investigations was made for different fluid bulk moduli, attachment location and flow coefficient. It achieved 32 and 16 percent damping ratio for first and second modes respectively. While, Krott, et al. [14] investigated the effect of tube compliance and volume change for these tubes. Their results showed that soft and thin tube bladders of F^2MC can provide damping. Miura, et al. [15] utilized an analytical model with Monte Carlo methods for vibration isolation in cantilever beams by using F^2MC tubes, with modifications on fluidic circuit dimensions and F^2MC tube attachment locations, the moment and shear transmission at the clamped end of the beam were reduced.

This paper sheds a new light on damping treatment of cantilever beams by using passive vibration control. It re-examines the diameter of F^2MC tubes by adding layer thickness ratios as a function of damping treatment for cantilevered structures. Within the framework of these criteria it evaluates two systems of F^2MC tubes in two different new categories, which has not been studied before. First is by bonding the two patches on the beam with examining the distance between them. And the latter is by bonding one patch on the beam and the other under the beam in various places. The mathematical model

presents a simple way for solving a complete system encompassing two F^2MC tube patches. They are connected separately with orifice through accumulator, filled with fluid. Each patch contains one F^2MC tube composed of three layers, the inner and middle layers are fiber reinforced laminate layers, with a liner outer layer. Both patches are integrated on the uniform cantilever beam. The system transfer function as a ratio of unit tip displacement per unit applied tip force was derived and plotted as Frequency Response Function (FRF).

2. Mathematical modelling

This study deals with integrating two patches of F^2MC tubes on the uniform cantilever beam, each consists of a single tube of three layered F^2MC tube. The first two respective layers are composite laminate fiber reinforced layers followed by an outer liner layer, surrounding a working fluid (glycerin). The patches are integrated above the beam, one after he other. Flow inside each of them is controlled by orifice through an accumulator. They are separated, the fluid inside them are not mixed together. they act as two separate fluidic systems to suppress vibrations that occur by beam bending with an action of applied point load.

2.1. Beam model

The Figures 1 and 2 show the patches of F2MC tubes. They assumed stiff and fixed very well on the beam. So, when the applied load (F) acts on the beam. They remain fixed in their positions during bending of the beam. This bending due to extension of the F2MC tubes in each system by an amount of (F_{t1}, and F_{t2}), and each results a formulation of a moments (M1) and (M2) in F2MC tubes bonding position as;

$$M1=F_{t1}\times d \tag{1}$$

$$M2=F_{t2}\times d \tag{2}$$

Using Euler-Bernoulli beam theory the governing equations of transverse displacement $y_{(x,t)}$ is formulated as:

$$m\frac{d^2y}{dt^2}+B\frac{dy}{dt}+EI\frac{d^4y}{dx^4}=0 \text{ for } x\in(0,L). \tag{3}$$

Where

$$m=\rho\times b\times h \tag{4}$$

Taking the Laplace transform, and solving for zero initial conditions

$$ms^2Y+BsY+EI\frac{d^4Y}{dx^4}=0 \tag{5}$$

And rearranging

$$\frac{d^4Y}{dx^4}-\beta^4Y(x)=0 \tag{6}$$

Where

$$\beta^4=\frac{s^2m+sB}{EI} \tag{7}$$

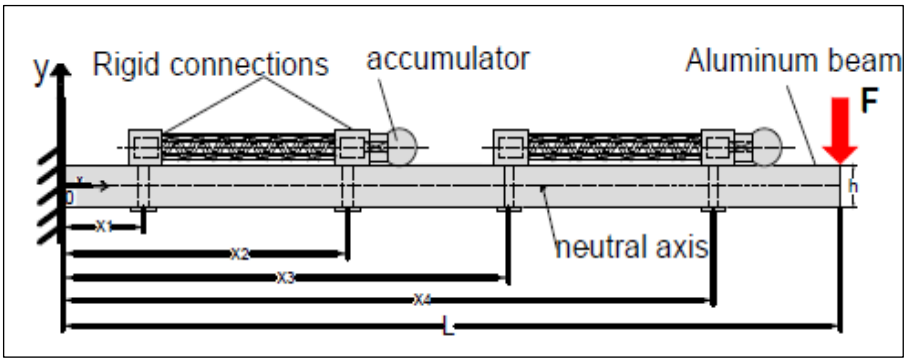

Fig.1 F²MC tubes Integrated on cantilever beam.

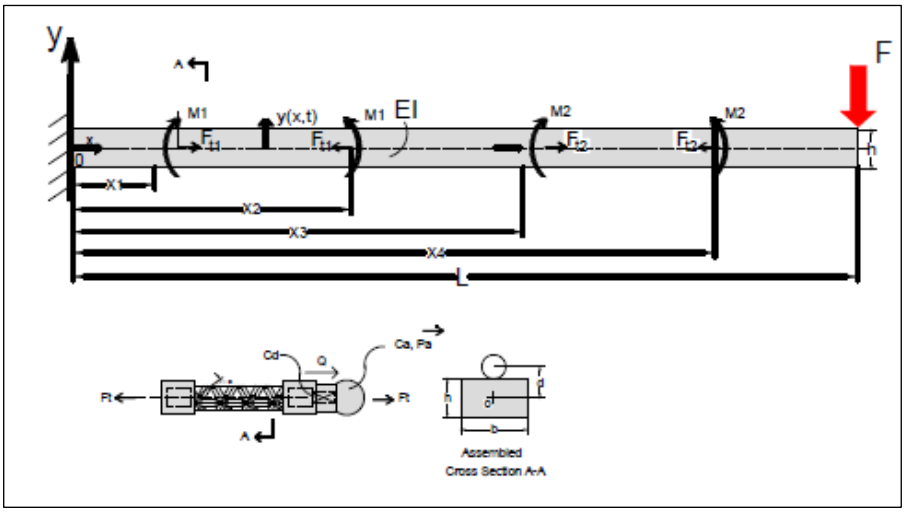

Fig. 2 Free body diagram of cantilever beam with integrated F2MC tubes, explaining forces, moments and attaching tubes locations on it.

The generalized solution of the beam has five domains:

$$Y=\begin{cases} Y1(x,s)=A1\sin\beta x+A2\cos\beta x+A3\sinh\beta x+A4\cosh\beta x, \text{ for } x\in(0,x_1) \\ Y2(x,s)=B1\sin\beta x+B2\cos\beta x+B3\sinh\beta x+B4\cosh\beta x, \text{ for } x\in(x_1,x_2) \\ Y3(x,s)=C1\sin\beta x+C2\cos\beta x+C3\sinh\beta x+C4\cosh\beta x \text{ , for } x\in(x_2,x_3) \\ Y4(x,s)=D1\sin\beta x+D2\cos\beta x+D3\sinh\beta x+D4\cosh\beta x, \text{ for } x\in(x_3, x_4) \\ Y5(x,s)=E1\sin\beta x+E2\cos\beta x+E3\sinh\beta x+E4\cosh\beta x, \text{ for } x\in(x_4, L) \end{cases} \quad (8)$$

The constants An, Bn, Cn Dn, and En for(n=1, 2, 3, 4) are found by using beam boundary conditions, [16]:

In the left side of the beam (x=0) the beam is

clamped, so

$$Y1(0,s)=0, \quad (9)$$

$$Y1'(0,s)=0. \quad (10)$$

Moment balance at $x=x_1$

$$EI(Y2''(x_1,s)-Y1''(x_1,s)=M1(s) \quad (11)$$

where $M(s)=\mathcal{L}M(t)$, by continuity

$$Y1(x_1,s)=Y2(x_1,s) \quad (12)$$

$$Y1'(x_1,s)=Y2'(x_1,s) \quad (13)$$

$$Y1'''(x_1,s)=Y2'''(x_1,s) \quad (14)$$

Moment balance at $x=x_2$ led to

$$EI(Y2''(x_2,s)-Y3''(x_2,s)=M1(s) \quad (15)$$

and the continuity due to

$$Y2(x_2,s)=Y3(x_2,s) \quad (16)$$

$$Y2'(x_2,s)=Y3'(x_2,s) \quad (17)$$

$$Y2'''(x_2,s)=Y3'''(x_2,s) \quad (18)$$

Moment balance at x=x3

$$EI(Y4''(x_3,s)-Y3''(x_3,s)=M2(s) \quad (19)$$

and the continuity due to

$$Y3(x_3,s)=Y4(x_3,s) \quad (20)$$

$$Y3'(x_3,s)=Y4'(x_3,s) \quad (21)$$

$$Y3'''(x_3,s)=Y4'''(x_3,s) \quad (22)$$

Moment balance at $x=x_4$

$$EI(Y4''(x_4,s)-Y5''(x_4,s)=M2(s) \quad (23)$$

and continuity gives

$$Y4(x_4,s)=Y5(x_4,s) \quad (24)$$

$$Y4'(x_4,s)=Y5'(x_4,s) \quad (25)$$

$$Y4'''(x_4,s)=Y5'''(x_4,s) \quad (26)$$

At free end, x=L

$$EIY5'''(L,s)=F(s) \quad (27)$$

$$EIY5''(L,s)=0 \quad (28)$$

2.2. Three layered F²MC tube model

Figure (1) shows that the patches are integrated on the beam. Each patch consist of a pair of F²MC tubes connected in parallel. The F²MC tube is modelled as a structure that consists of three coaxial boundless length hollow cylinders perfectly bonded together: the inner and middle cylinders are FMC laminate, both are made from polyacrylonitrile-based carbon fiber. They are orthotropic, with reinforcing fibres oriented at $\pm\alpha$ to the axial direction of the tube; the outer liner cylinder is made from polyurethane (Fig.3). Each cylinder represents a layer, and the radii of layers from inside to outside are c_1, c_2, c_3 and c_4 respectively. The axial force exerted on the F²MC tube balances the force on the individual tube layers,

$$T=T_1+T_2+T_3 \quad (29)$$

For two layered F²MC tubes, the axial force can be found by summing only T_1 and T_2.

2.2.1. Inner and middle layers

Figure 3 highlights that the FMC inner layer is subjected to axial force (T_1), internal surface pressure (p_o) and external surface pressure(p_1). The axial force is:

$$T_1=2\pi\int_{c_1}^{c_2}\sigma_z^i c\,dc, \tag{30}$$

Where σ_z^i represents the axial stress in the inner layer.

Furthermore, Lekhnitskii's elasticity solution for homogenous orthotropic cylinders was used to find the generalized stress distributions[17], as:

$$\sigma_r^i=\frac{p_0a^{k+1}-p_1}{1-a^{2k}}\mu^{k-1}+\frac{p_1a^{k-1}-p_0}{1-a^{2k}}a^{k+1}\mu^{-k-1}+AhK_1, \tag{31}$$

$$\sigma_\theta^i=\frac{p_0a^{k+1}-p_1}{1-a^{2k}}k\mu^{k-1}-\frac{p_1a^{k-1}-p_0}{1-a^{2k}}ka^{k+1}\mu^{-k-1}+AhK_2, \tag{32}$$

$$\sigma_z^i=A-\frac{1}{b_{33}}\left(b_{13}\sigma_r^i+b_{23}\sigma_\theta^i\right), \tag{33}$$

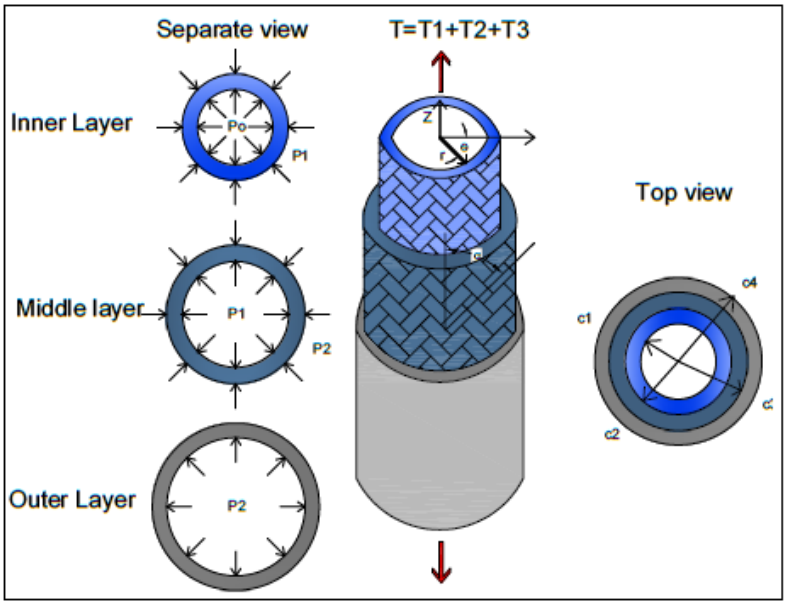

Fig. 3 Sketch of F²MC tube with dimensions and loads on layers.

Where r, θ and z indicate radial, hoop and axial directions (Fig.3),

$$a=\frac{c_1}{c_2}, \tag{34}$$

$$\mu=\frac{c}{c_2}, \tag{35}$$

$$k=\sqrt{\frac{\beta_{11}}{\beta_{22}}}, \tag{36}$$

$$h=\frac{b_{23}-b_{13}}{\beta_{11}-\beta_{22}}, \tag{37}$$

$$\beta_{11}=b_{11}-\frac{b_{13}^2}{b_{33}}, \quad (38)$$

$$\beta_{22}=b_{22}-\frac{b_{23}^2}{b_{33}}, \quad (39)$$

$$K_1=1-\frac{1-a^{k+1}}{1-a^{2k}}\mu^{k-1}-\frac{1-a^{k-1}}{1-a^{2k}}a^{k+1}\mu^{-k-1}], \quad (40)$$

$$K_2=1-\frac{1-a^{k+1}}{1-a^{2k}}k\mu^{k-1}+\frac{1-a^{k-1}}{1-a^{2k}}ka^{k+1}\mu^{-k-1}], \quad (41)$$

The b_{ij}terms are three-dimensional effective compliance constants found from the homogenous properties of the inner layer in the cylindrical coordinate system [18, 19]. The transversely isotropic unidirectional reinforced $(+\alpha)$ and $(-\alpha)$ sub-layers are assumed for calculating the homogenous properties of $\pm\alpha$ composite layers. Therefore, the layers have five independent elastic constants: longitudinal and transverse modulus of elasticity E11, E22, Poisson's ratio $\nu_{12}$and ν_{23} and longitudinal shear modulus of elasticity G_{12}. Solving the equations (30-33) lead to finding the parameter (A) as a function of (T_1, p_0 and p_1). The strain distributions for the inner composite layer are:

$$\varepsilon_r^i=b_{11}\sigma_r^i+b_{12}\sigma_\theta^i+b_{13}\sigma_z^i, \quad (42)$$

$$\varepsilon_\theta^i=b_{12}\sigma_r^i+b_{22}\sigma_\theta^i+b_{23}\sigma_z^i, \quad (43)$$

$$\varepsilon_z^i=b_{13}\sigma_r^i+b_{23}\sigma_\theta^i+b_{33}\sigma_z^i, \quad (44)$$

Similarly, the axial force (T_2), stresses $(\sigma_r^m, \sigma_\theta^m, \sigma_z^m)$ and strains $(\varepsilon_r^m, \varepsilon_\theta^m, \varepsilon_z^m)$ for the middle reinforced layer are found by replacing $(T_1, p_0, p_1, c_1$ and $c_2)$ with $(T_2, p_1, p_2, c_2$ and $c_3)$ respectively in Eqs. (30-44).

2.2.2. Outer layer

This layer is modelled as an infinitely long isotropic hollow cylinder with an axial force (T_3), inside and outside surface pressures (p_2) and $(p_3 = 0)$ (Fig. 3). Therefore, relying on [20], the stress distributions are:

$$\sigma_r^o=\frac{p_2c_3^2-p_3c_4^2}{c_4^2-c_3^2}-\frac{c_3^2c_4^2(p_2-p_3)}{c^2(c_4^2-c_3^2)}, \quad (45)$$

$$\sigma_\theta^o=\frac{p_2c_3^2-p_3c_4^2}{c_4^2-c_3^2}+\frac{c_3^2c_4^2(p_2-p_3)}{c^2(c_4^2-c_3^2)}, \quad (46)$$

$$\sigma_z^o=\frac{T_3}{\pi(c_4^2-c_3^2)}, \quad (47)$$

The strains in each direction can be obtained by using Hooke's law:

$$\varepsilon_r^o=\frac{1}{E_o}[\sigma_r^o-\nu_o(\sigma_\theta^o+\sigma_z^o)], \quad (48)$$

$$\varepsilon_\theta^o=\frac{1}{E_o}[\sigma_\theta^o-\nu_o(\sigma_r^o+\sigma_z^o)], \quad (49)$$

$$\varepsilon_z^o=\frac{1}{E_o}[\sigma_z^o-\nu_o(\sigma_\theta^o+\sigma_r^o)], \quad (50)$$

Where (E_oE_o) and (ν_o) are Young's modulus of elasticity and Poisson's ratio for polyurethane respectively.

2.3. Equilibrium equations

In this model, each F2MC patch follows a plain strain solution, as the beam extends uniformly in an axial direction, therefore:

$$\varepsilon_z^i=\varepsilon_z^m, \quad (51)$$

$$\varepsilon_z^m=\varepsilon_z^o. \quad (52)$$

At the interface between any two layers the hoop strains are identical,

$$\varepsilon_\theta^i\big|_{c=c_2}=\varepsilon_\theta^m\big|_{c=c_2} \quad (53)$$

$$\varepsilon_\theta^m\big|_{c=c_3}=\varepsilon_\theta^o\big|_{c=c_3} \quad (54)$$

The axial force on each F2MC patch balances the loads on the end of the F2MC tube,

$$T_1=\frac{Ft_1}{N}+p_o\pi c_1^2 \quad (55)$$

$$T_2=\frac{Ft_2}{N}+p_o\pi c_1^2 \quad (56)$$

Where (p_o) is fluid pressure inside the tubes and (N) is the number of tubes. By given geometry and material properties (Table 1), the axial and hoop strains of the inner layer can be calculated by solving Eq. (51-56) as functions of (T and p_0) as

$$\varepsilon_{\theta 1}\big|_{r=c_1}=\emptyset_1 T_1+\emptyset_2 p_0 \quad (57)$$

$$\varepsilon_{\theta 2}\big|_{r=c_1}=\emptyset_1 T_2+\emptyset_2 p_0 \quad (58)$$

And

$$\varepsilon_{z1}=\emptyset_3 T_1+\emptyset_4 p_0 \quad (59)$$

$$\varepsilon_{z2}=\emptyset_3 T_2+\emptyset_4 p_0 \quad (60)$$

where $\varepsilon_{\theta 1}, \varepsilon_{\theta 2}, \varepsilon_{z1}$, and ε_{z2} are strains in hub and axial directions for first and second patches respectively, and $\emptyset_1, \emptyset_2, \emptyset_3$ and $\emptyset_4$ are constants representing the geometry and material properties of the F2MC tubes for all patches.

Table 1 Model parameters and material properties of F^{2}MC tubes

Parameter	Symbol	Quantity
Fiber reinforced layer		
Longitudinal modulus of elasticity (GPa)	E_{11}	40
Transverse modulus of elasticity (MPa)	E_{22}	1.8
Poisons ratio	v12	0.33
Poisons ratio	v23	0.39
Modulus of rigidity (MPa)	G_{12}	1.4
Fiber angle (°)	α	±27
Liner Layer		
Modulus of elasticity (MPa)	E_o	11MPa
Poisons ratio	v_o	0.498
F^{2}MC tube geometry and integration points		
Inner layer internal radius(mm)	c1	1 mm, (0.5-10) mm
Middle layer internal radius (mm)	c2	1.7 c_1
Outer layer internal radius(mm)	c3	1.8 c_1
Outer radius (mm)	c4	2.105 c_1

Length of first patch of F²MC tube's (mm)	L_{FMC1}	x_1-x_2,
Length of second patch of F²MC tubes(mm)	L_{FMC2}	x_3-x_4
Attaching points:	x_1	0
	x_2	75mm
	x_3	(110-140) mm
	x_4	(185-215) mm
Beam geometry		
Hight (mm)	h	1.6
Width (mm)	b	26
Length (mm)	L	310
Beam material	Aluminium	
Modulus of elasticity (GPa)	E	70
Damping constant (N s/m)	C	0.2
Density (kg/M^3)	ρ	2700
Fluid properties		
Type of fluid	glycerine	
Density (kg/M^3)	ρ	1260
Bulk modulus (gpa)	B	4.35
Accumulator capacitance (m3/Pa)	Ca	1.5×10^{-9}
Flow coefficient (m3/s Pa)	C_d	2×10^{-13}

2.4. Fluid Behavior

The study includes multi-F²MC patch model in a closed valve scenario. It is assumed that the tubes are filled with fluid, which are tight with no differential pressure with the bulk modulus (B) and volume of (V_i). When the force (F) is applied, the volume of the F²MC tubes changes by the amount of (ΔV_f) with the formation of (F_{t1}, and F_{t2}). Depending on the volume change, the fluid differential pressure changes from zero to (p_0). For first patch, this can be expressed as:

$$(\frac{\Delta V_f}{V_{i1}})B=-p_0, \quad (61)$$

But the volume change of F²MC tube is defined as:

$$\Delta V_1=V_1-V_{i1}, \quad (62)$$

Where

$$V_1=\pi\left[\left(1+\varepsilon_{\theta 1}|_{r=c_1}\right)c_1\right]^2(x2-x1)(1+\varepsilon_z), \quad (63)$$

$$V_{i1}=\pi c_1^2(x2-x1). \quad (64)$$

For second patch, the procedure is the same only the bonding positions are changed:

$$\Delta V_2=V_2-V_{i2}, \quad (65)$$

$$V_2=\pi\left[\left(1+\varepsilon_{\theta 2}|_{r=c_1}\right)c_1\right]^2(x4-x3)(1+\varepsilon_z), \quad (66)$$

$$V_{i2}=\pi c_1^2(x4-x3). \quad (67)$$

Then, the volume ratio for each F²MC patch can be written as:

$$\frac{\Delta V_1}{V_{i1}}=\frac{V_{i1}-V_1}{V_{i1}}\cong\varepsilon_{z1}+2\varepsilon_{\theta 1}|_{r=c_1}, \quad (68)$$

$$\frac{\Delta V_2}{V_{i2}}=\frac{V_{i2}-V_2}{V_{i2}}\cong \varepsilon_{z2}+2\varepsilon_{\theta 2}|_{r=c_1} \quad (69)$$

The fluid volume that is pumped out of the first and second patches, which are composed of (N) tubes, was assumed as the fluid volume flow rate and expressed as

$$Q_{v1}= -N(\Delta V_1-\Delta V_f). \quad (70)$$

$$Q_{v2}= -N(\Delta V_2-\Delta V_f). \quad (71)$$

By substituting each of ΔV_f and $\Delta V_1$and ΔV_2 from equations (61), (62) and (65) respectively, yields

$$\dot{Q}_{v1}=NF_Q\dot{T}+NG_Q\dot{p_0} = \dot{Q}_{v2} \quad (72)$$

Where

$$G_Q=-(2\emptyset_1+\emptyset_3)V_{in} \quad (73)$$

$$F_Q=-(\emptyset_2+2\emptyset_4+\frac{1}{B})V_{in} \quad (74)$$

here $V_{in} = V_{i1}$ or V_{i2} , depending on the selected patch.

As the fluids inside both patches are the same type with the same configuration, the fluid volume flow rate balances the change in fluid pressure inside the orifice and accumulator by,

$$Q_v=C_d(p_0-p_A) \quad (75)$$

And

$$Q_v=C_a\dot{p_A} \quad (76)$$

Where (p_A) is the internal pressure of the accumulator, (C_d) the flow coefficient and (C_a) is the accumulator capacity.

2.5. Over all system's transfer function

The transfer function of patches can be determined by the ratio of the axial strain to the axial force by solving each of equations (55), (59), (72), (75), and (76), also (56), (60), (72), (75), and (76) in the Laplace domain with zero initial conditions for first and second patches respectively as follows:

$$\varepsilon_{z1}(s)= G_p(s)F_{t1}(s), \quad (77)$$

$$\varepsilon_{z2}(s)= G_p(s)F_{t2}(s) \quad (78)$$

Where

$$G_p(s)=\frac{(c_as+c_d)(\emptyset_3F_Q-\emptyset_4G_Q)-\theta_3c_ac_d/N}{N(c_as+c_d)(F_Q+\pi c_1^2G_Q)-c_ac_d} \quad (79)$$

As required by Lekhnitskii's theory of elasticity [17], the patches stretch uniformly in an axial direction, and the total F2MC tube patch elongation can be calculated as,

$$\Delta L_1(s)=L_{FMC1}\varepsilon_{z1}(s)= -d(\frac{dY_2(s)}{dx2}-\frac{dY_2(s)}{dx1}), \quad (80)$$

$$\Delta L_2(s)=L_{FMC2}\varepsilon_{z2}(s)= -d(\frac{dY_4(s)}{dx4}-\frac{dY_4(s)}{dx3}), \quad (81)$$

Where $L_{FMC1}=(x_2-x_1)$, and $L_{FMC2}=(x_4-x_3)$

Substituting (Ft1) and (d) in Eqs. (77, 80) into Eq. (1) then solving for moment (M1), and substituting (Ft2) and (d) in Eqs. (78, 81) into Eq. (2) then solving for moment (M2), yield the following equations:

$$M1(s)=\frac{1}{U1(s)}\left[\frac{dY_2(s)}{dx2}-\frac{dY_2(s)}{dx1}\right],$$
$$M2(s)=\frac{1}{U2(s)}\left[\frac{dY_4(s)}{dx4}-\frac{dY_4(s)}{dx3}\right], \quad (82)$$

Where

$$U1(s)=\frac{L_{FMC1}}{d^2}G_p(s)\ ,\ U2(s)=\frac{L_{FMC2}}{d^2}G_p(s) \quad (83)$$

Now, substituting equation (82) into the constant's equations (9 –28)the following expression can be obtained:

$$J\ w=b\ F(s), \quad (84)$$

Where

$$J=\begin{bmatrix}
0 & 1 & 0 & 1 & 0 & 0 & 0 & 0 & 0 & 0 & 0 & 0 & 0 & 0 & 0 & 0 & 0 & 0 & 0 & 0\\
1 & 0 & 1 & 0 & 0 & 0 & 0 & 0 & 0 & 0 & 0 & 0 & 0 & 0 & 0 & 0 & 0 & 0 & 0 & 0\\
J_{31} & J_{32} & J_{33} & J_{34} & J_{35} & J_{36} & J_{37} & J_{38} & 0 & 0 & 0 & 0 & 0 & 0 & 0 & 0 & 0 & 0 & 0 & 0\\
J_{41} & J_{42} & J_{43} & J_{44} & J_{45} & J_{46} & J_{47} & J_{48} & 0 & 0 & 0 & 0 & 0 & 0 & 0 & 0 & 0 & 0 & 0 & 0\\
J_{51} & J_{52} & J_{53} & J_{54} & J_{55} & J_{56} & J_{57} & J_{58} & 0 & 0 & 0 & 0 & 0 & 0 & 0 & 0 & 0 & 0 & 0 & 0\\
J_{61} & J_{62} & J_{63} & J_{64} & J_{65} & J_{66} & J_{67} & J_{68} & 0 & 0 & 0 & 0 & 0 & 0 & 0 & 0 & 0 & 0 & 0 & 0\\
0 & 0 & 0 & 0 & J_{75} & J_{76} & J_{77} & J_{78} & J_{79} & J_{710} & J_{711} & J_{712} & 0 & 0 & 0 & 0 & 0 & 0 & 0 & 0\\
0 & 0 & 0 & 0 & J_{85} & J_{86} & J_{87} & J_{88} & J_{89} & J_{810} & J_{811} & J_{812} & 0 & 0 & 0 & 0 & 0 & 0 & 0 & 0\\
0 & 0 & 0 & 0 & J_{95} & J_{96} & J_{97} & J_{98} & J_{99} & J_{910} & J_{911} & J_{912} & 0 & 0 & 0 & 0 & 0 & 0 & 0 & 0\\
0 & 0 & 0 & 0 & J_{105} & J_{106} & J_{107} & J_{108} & J_{109} & J_{1010} & J_{1011} & J_{1012} & 0 & 0 & 0 & 0 & 0 & 0 & 0 & 0\\
0 & 0 & 0 & 0 & 0 & 0 & 0 & 0 & J_{119} & J_{1110} & J_{1111} & J_{1112} & J_{1113} & J_{1114} & J_{1115} & J_{1116} & 0 & 0 & 0 & 0\\
0 & 0 & 0 & 0 & 0 & 0 & 0 & 0 & J_{129} & J_{1210} & J_{1211} & J_{1212} & J_{1213} & J_{1214} & J_{1215} & J_{1216} & 0 & 0 & 0 & 0\\
0 & 0 & 0 & 0 & 0 & 0 & 0 & 0 & J_{139} & J_{1310} & J_{1311} & J_{1312} & J_{1313} & J_{1314} & J_{1315} & J_{1316} & 0 & 0 & 0 & 0\\
0 & 0 & 0 & 0 & 0 & 0 & 0 & 0 & J_{149} & J_{1410} & J_{1411} & J_{1412} & J_{1413} & J_{1414} & J_{1415} & J_{1416} & 0 & 0 & 0 & 0\\
0 & 0 & 0 & 0 & 0 & 0 & 0 & 0 & 0 & 0 & 0 & 0 & J_{1513} & J_{1514} & J_{1515} & J_{1516} & J_{1517} & J_{1518} & J_{1519} & J_{1520}\\
0 & 0 & 0 & 0 & 0 & 0 & 0 & 0 & 0 & 0 & 0 & 0 & J_{1613} & J_{1614} & J_{1615} & J_{1616} & J_{1617} & J_{1618} & J_{1619} & J_{1620}\\
0 & 0 & 0 & 0 & 0 & 0 & 0 & 0 & 0 & 0 & 0 & 0 & J_{1713} & J_{1714} & J_{1715} & J_{1716} & J_{1717} & J_{1718} & J_{1719} & J_{1720}\\
0 & 0 & 0 & 0 & 0 & 0 & 0 & 0 & 0 & 0 & 0 & 0 & J_{1813} & J_{1814} & J_{1815} & J_{1816} & J_{1817} & J_{1818} & J_{1819} & J_{1820}\\
0 & 0 & 0 & 0 & 0 & 0 & 0 & 0 & 0 & 0 & 0 & 0 & 0 & 0 & 0 & 0 & J_{1917} & J_{1918} & J_{1919} & J_{1920}\\
0 & 0 & 0 & 0 & 0 & 0 & 0 & 0 & 0 & 0 & 0 & 0 & 0 & 0 & 0 & 0 & J_{2017} & J_{2018} & J_{2019} & J_{2020}
\end{bmatrix},\ w=\begin{bmatrix}A1\\A2\\A3\\A4\\B1\\B2\\B3\\B4\\C1\\C2\\C3\\C4\\D1\\D2\\D3\\D4\\E1\\E2\\E3\\E4\end{bmatrix},\ b=\begin{bmatrix}0\\0\\0\\0\\0\\0\\0\\0\\0\\0\\0\\0\\0\\0\\0\\0\\0\\0\\1\\\frac{}{EI\beta^3}\\0\end{bmatrix} \quad (85)$$

And

J_{31}=U1EIβSβx$_1$ J_{41}=Sβx_1 J_{51} = Cβx_1 J_{61}= − Cβx$_1$

J_{32}=U1EIβCβx$_1$ J_{42}=Cβx_1 J_{52} = −Sβx_1 J_{62}=Sβx$_1$

J_{33}= − U1EIβShβx$_1$ J_{43}=Shβx_1 J_{53} = Chβx$_1$ J_{63}=Chβx$_1$

J_{34}= − U1EIβChβx$_1$ J_{44}=Chβx_1 J_{54} = Shβx$_1$ J_{64}=Shβx$_1$

J_{35}= − U1EIβSβx$_1$ − Cβx$_2$+Cβx$_1$ J_{45}= − Sβx_1 J_{55} = −Cβx_1 J_{65}=Cβx$_1$

J_{36}= − U1EIβCβx$_1$+Sβx$_2$ − Sβx$_1$ J_{46}= − Cβx_1 J_{56} = Sβx_1 J_{66}= − Sβx$_1$

J_{37}=U1EIβShβx$_1$ − Chβx$_2$+Chβx$_1$ J_{47}= − Shβx_1 J_{57} = −Chβx$_1$ J_{67}= − Chβx$_1$

J_{38}=U1EIβChβx$_1$ − Shβx$_2$+Shβx$_1$ J_{48}= − Chβx_1 J_{58} = −Shβx_1 J_{68}= − Shβx$_1$

J_{75}= − U1EIβSβx$_2$ − Cβx$_2$+Cβx$_1$ J_{85} = Sβx$_2$ J_{95}=Cβx$_2$ J_{105}= − Cβx$_2$

J_{76}= − U1EIβCβx$_2$+Sβx$_2$ − Sβx$_1$ J_{86} = Cβx$_2$ J_{96}= − Sβx$_2$ J_{106}=Sβx$_2$

J_{77}=U1EIβShβx$_2$ − Chβx$_2$+Chβx$_1$ J_{87} = Shβx$_2$ J_{97}=Chβx$_2$ J_{107}=Chβx$_2$

J_{78}=U1EIβChβx$_2$ − Shβx$_2$+Shβx$_1$ J_{88} = Chβx$_2$ J_{98}=Shβx$_2$ J_{108}=Shβx$_2$

J_{79}= U1EIβSβx$_2$ J_{89} = −Sβx$_2$ J_{99}= − Cβx$_2$ J_{109}= Cβx$_2$

J_{710}= U1EIβCβx$_2$ J_{810} = −Cβx$_2$ J_{910}=Sβx$_2$ J_{1010}= − Sβx$_2$

J_{711}= − U1EIβShβx$_2$ J_{811} = −Shβx$_2$ J_{911}= − Chβx$_2$ J_{1011}= − Chβx$_2$

J_{712}= − U1EIβChβx$_2$ J_{812} = −Chβx$_2$ J_{912}= − Shβx$_2$ J_{1012}= − Shβx$_2$

J_{119} = U2EIβSβx$_3$ J_{129}=Sβx$_3$, J_{139}=Cβx$_3$ J_{149} = −Cβx$_3$

J_{1110} = U2EIβCβx$_3$ J_{1210}=Cβx$_3$ J_{1310}= − Sβx$_3$ J_{1410} = Sβx$_3$

J_{1111} = −U2EIβShβx$_3$ J_{1210}=Shβx$_3$ J_{1311}=Chβx$_3$ J_{1411} = Chβx$_3$

J_{1112} = −U2EIβChβx$_3$ J_{1212}=Chβx$_3$ J_{1312}=Shβx$_3$ J_{1412} = Shβx$_3$

J_{1113} = −U2EIβSβx$_3$ − Cβx$_4$ + Cβx$_3$ J_{1213}= − Sβx$_3$ J_{1313}= − Cβx$_3$ J_{1413} = Cβx$_3$,

J_{1114} = −U2EIβCβx$_3$ + Sβx$_4$ − Sβx$_3$ J_{1214}= − Cβx$_3$ J_{1314}= Sβx$_3$ J_{1414} = −Sβx$_3$

J_{1115} = U2EIβShβx$_3$ − Chβx$_4$ + Chβx$_3$ J_{1215}= − Shβx$_3$ J_{1315}= − Chβx$_3$ J_{1415} = −Chβx$_3$

J_{1116} = U2EIβChβx$_3$ − Shβx$_4$ + Shβx$_3$ J_{1216}= − Chβx$_3$ J_{1316}= − Shβx$_3$ J_{1416} = −Shβx$_3$

J_{1513}= − U2EIβSβx$_4$ − Cβx$_4$ + Cβx$_3$ J_{1613}=Sβx$_4$ J_{1713}=Cβx$_4$ J_{1813}= − Cβx$_4$

J_{1514}= − U2EIβCβx$_4$ + Sβx$_4$ − Sβx$_3$ J_{1614}=Cβx$_4$ J_{1714}= − Sβx$_4$ J_{1814}=Sβx$_4$

J_{1515}=U2EIβShβx$_4$ − Chβx$_4$ + Chβx$_3$ J_{1615}=Shβx$_4$ J_{1715}=Chβx$_4$ J_{1815}=Chβx$_4$

J_{1516}=U2EIβChβx_4 − Shβx_4 + Shβx_3 J_{1616}=Chβx_4 J_{1716}=Shβx_4 J_{1816}=Shβx_4

J_{1517}=U2EIβSβx_4 J_{1617}= − Sβx_4 J_{1717}= − Cβx_4 J_{1817}= Cβx_4

J_{1518}=U2EIβCβx_4 J_{1618}= − Cβx_4 J_{1718}= Sβx_4 J_{1818}= − Sβx_4

J_{1519}= − U2EIβShβx_4 J_{1619}= − Shβx_4 J_{1719}= − Chβx_4 J_{1819}= − Chβx_4

J_{1520}= − U2EIβChβx_4 J_{1620}= − Chβx_4 J_{1720}= − Shβx_4 J_{1820}= − Shβx_4

J_{1917}= − EICβL J_{2017}= − EISβL

J_{1918}=EISβL J_{2018}= − EICβL

J_{1919}=EIChβL J_{2019}=EIShβL

J_{1920}=EIShβL J_{2020}=EIChβL

Where S, C, Sh, Ch, U1, and U2 are sin, cos, sinh, cosh, U1(s), and U2(s) respectively.

The total deflection at the free end of the beam is

$$Y(L,s)= E1\sin\beta L+E2\cos\beta L+E3\sinh\beta L+E4\cosh\beta L \quad (86)$$

In addition, the overall transfer function of the F^2MC structure is

$$\frac{Y(L,s)}{F(s)}=a_w J^{-1} b=H(s) \quad (87)$$

With
a_w=[0 0 0 0 0 0 0 0 0 0 0 0 0 0 0 0 sinβL cosβL sinhβL coshβL], and the FRF is represented by |H(jω)|.

3. Model validation

As producing F^2MC tubes samples are difficult. It requires sophisticated devices because of their size and layer thickness, the derived model validated theoretically by performing some illustrative examples and the results were compared with the existing data available in the literature to demonstrate the accuracy of the present model. As an example, comparisons are made between the FRF plot obtained from the previous studies [13] for a patch of F^2MC tubes integrated on the cantilever beam (Fig. 4). It could be seen, the present results are in well agreement with similar ones available in previous studies in the reference, which had been agreed with their experimental validations. This agreement improved the proposal of a new model, strong enough to be used for future studies. Then this model has been modified for two patches of the tubes integrated on the beam instead of one.

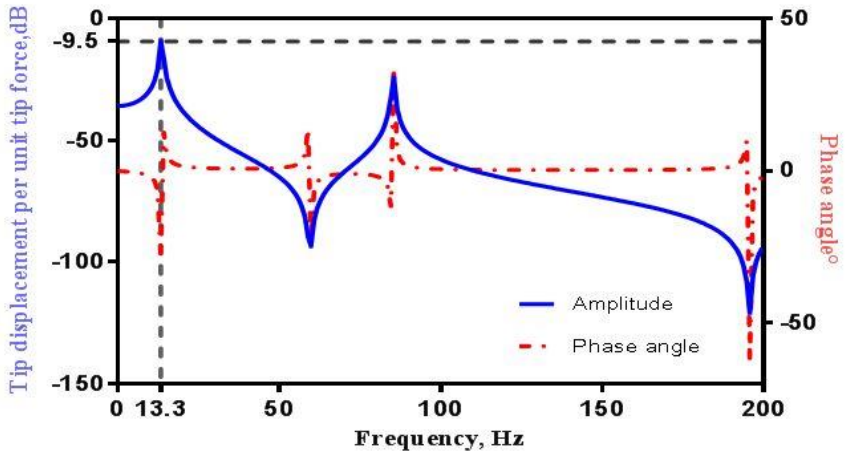

Fig. 4 Frequency response plot for studied model for comparison purpose [13].

4. Parametric studies

4.1 Studying the integration points of the second patch

In a previous study of F^2MC tubes, the integration points of a single patch of F^2MC was concluded with sensible reduction in amplitude of vibration in FRF plot. This was obtained by locating the first bonding position (x_1) on the fixed end of the beam [13]. Because in this point maximum moment was recorded. This study aimed to achieve higher reductions in amplitude of resonance in the first mode shape, by integrating two similar patches ($L_{FMC1}=L_{FMC2}=75$ mm) of F^2MC tubes. The first patch's integration point ($x_1=0$, $x_2=75$mm) is fixed, because of achieved results in the literature. While, the second patch's integration points have been examined. The study started with integrating it on the free end of the beam ($x_3=235$, $x_4=310$) then these values were reduced enough to make the two patches close to each other. The minimum possible studied distance between the patches was (35 mm). As the patches being closer to each other more damping was obtained, because as the patches are bonded on the positions near to fixed end of the beam. The transverse vibrations that obtained by beam bending will lead to increase in the fluid flow into the patches then the volume of the tubes is expanded and damping would increase. Whereas, when the second patch was so far from the first patch (on the free end), the fluid entering into the second patch is eliminated, thus the beam damped under the action of only one patch, and the undamped vibrations were recorded. Figure 5, shows the reductions in the first mode shape's resonance amplitude with reducing the distance (x) between the patches. The distance (x) is directly proportional with amplitude of resonance and inversely proportional with frequency of resonance. This result was supported by other researchers, [21]. In contrast, by reducing the distance between the two F^2MC tube patches, the reduction achievement in first mode amplitude was 7.25dB with 4.55 Hz wider resonance frequency. The maximum reduction in pick amplitude was obtained with the smallest distance between the two patches, which was plotted by solid line in the Fig 5. With this distance, the recorded amplitude of first mode shape was -50.3dB, which is larger than the reductions recorded by Zhu et al. through getting benefit of inertia track length. [22]. The present model in this paper is more efficient in reducing vibrations with regard to sizes used, as compared with study done by Krott, et al. [14]. While comparing this result with reduction obtained by Multi Input Multi Output Linear Quadratic Gaussian Controller MIMI-LQG, the present reduction was greater than MIMO-LQG controller [5].

After fixing the distance between the patches, then the next step is examining the integration of the second patch under the beam with two configurations: in the same integration point with the first patch (x1=x3=0, x2=x4=75mm); and at the fixed distance (x=35mm) between the patches. The mathematical modelling of the system with patches under the beam follows the same procedure listed in section 2. Only their will be a change in sign of the second patches' transfer function Eqs. (82-83). It defines as $U2(s)=\frac{-L_{FMC2}}{d^2}G_p(s)$. This outline contributed significant vibration suppression in terms of the peak amplitude reduction in FRF during comparison with a patch contains pair of F2MC tubes [12], which was assumed as base line model in Fig. 6. The comparison of each studied cases with base line model shows that, the first configuration reduced first resonance amplitude by 9.44 dB, with a very small reduction in its frequency, whereas, the second configuration achieved significant reductions in both amplitudes and frequency of resonance in all mode shapes. As it can be notified from the Fig.6 the first mode shape's reductions in amplitude and frequency of resonance are 10.12 dB and 11.4Hz, respectively with second mode shape's overall gain reduction.

Authors in this study relating the resulted reductions to the positions that the patches have been integrated with the beam. In the first case study the second patches' bonding points comes in agreement with the results that previously discussed that vibration elimination by damper would be more powerful when dampers installed in the locations with maximum mode displacement happens,[23].

On the other hand, when the two configurations of integrating the patches under the beam are compared with a model of integrating the patches on the beam, the comparison result in Fig. 7 shows the similar responses in first mode shape between integrating the patches above and under the beam. In both cases the integration points were the same (x1=0, x2=75, x3=110, and x4=185 mm), the only difference was in the second patches' place (above or under the beam) which results in change in sign of Eq. (82-83) as explained before. As it can be notified from mathematical modelling, in the case of bonding the patches on the beam, both patches will elongate in the same direction and producing different moments, while in the case of integrating one above and the other under the beam, the second patch will act under compression which directly reduces the amplitudes of mode shapes, This change in the second patches transfer function might has direct effect on reducing the resonance amplitudes that recorded. Joining the F2MC tube patches above the beam is good for reducing amplitude of vibrations. In the case of using the tubes in low frequency range applications, integrating the patches as first configuration is better to be avoided, Fig.7. Furthermore, when a pair of F2MC tubes was used in each path and compared with previous case, when single tubes were used. The resulted plot shows that single tubes highlight lower amplitudes of resonance in all mode shapes as compared a pair of tubes. The reason of this behavior is due to the lower pressure generation of fluid inside the tubes, because the same amount of fluid would enter two tubes instead of one. The fluid distribution between the two tubes, directly reduced the amount of fluid flow entering each tube and minimizes the moments M1 and M2 that found in bonding points; following a resulted lower beam damping (Fig.8).

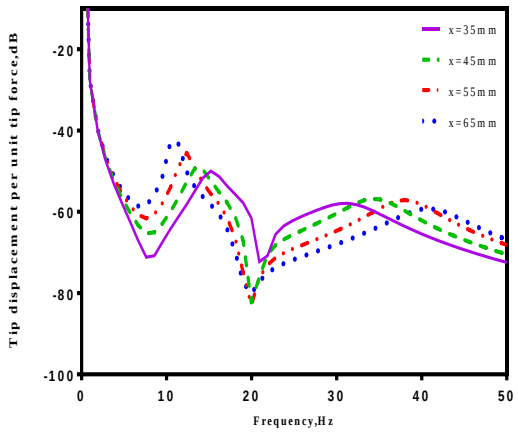

Fig. 5 Zoomed view for the first mode shape in FRF response of two patches bonded on the cantilever beam, the first patch fixed whereas the second patch's integration point was varied; solid line for the distance between the patches x=35mm, dashed for x=45mm, dash-dotted for x=55mm, and dotted for x=65mm.

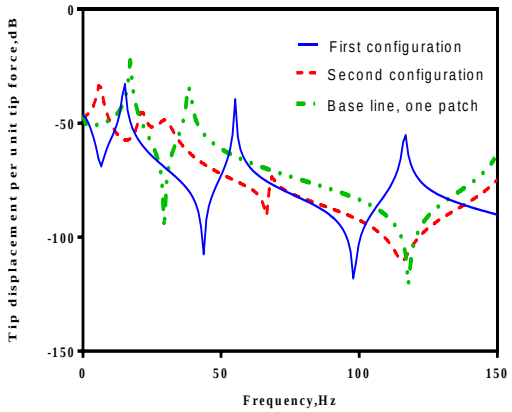

Fig. 6 FRF response of two patches integrated under the beam: 1st configuration (solid) on the same axis, $x_1=x_3=0$, $x_2=x_4=75mm$ and 2nd configuration (dashed), on the different axis, $x_1=0$, $x_2=75mm$, $x_3=110mm$ and $x_4=185mm$. Base line model (dash-doted), one patch of a pair F^2MC tubes bonded on the beam, x1=0, x2=150mm.

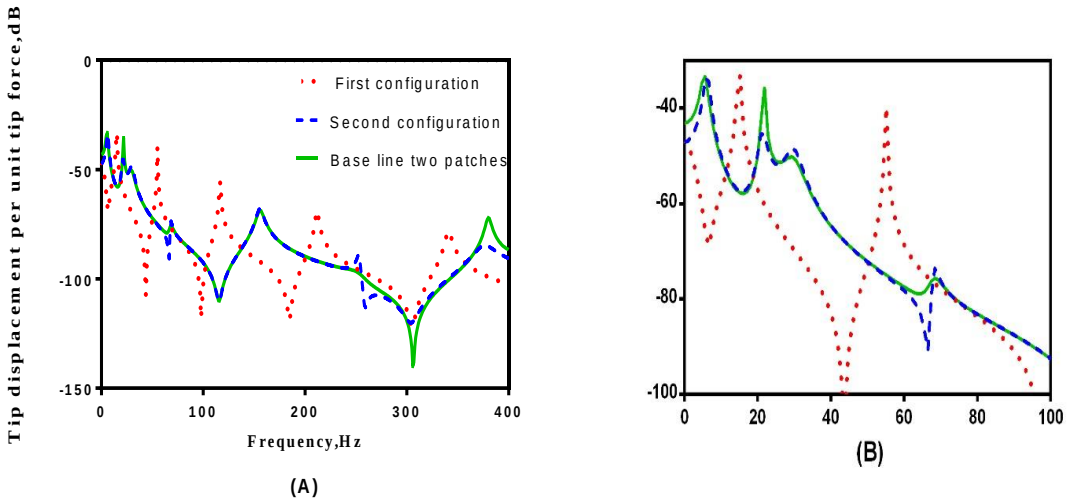

Figure 7 FRF response comparison between the two configurations with a model of two patches integrated on the beam: (A) Normal view, (B) zoomed view of 1st and 2nd mode shapes.

4.2 The size of F²MC tubes

This case deals with the second configuration model when the patches bonded one above and the other under the beam with bonding locations $x_1 = x_3 = 0; \text{and}\ \ x2 = x4 = 75\text{mm}$, respectively. Fabrication of F2MC tubes with a very small size are practically difficult [14]. For this reason, the authors examined bigger sizes that practically possible to be produced. The F2MC tubes with different sizes have been examined, the tubes' inner radius from (0.5-10 mm) are studied, for each value of inner radius (c1), the other radii, c_2, c_3, and c_4 were selected as: $1.7c_1$, $1.8c_1$, and $2.105c_1$ respectively. Figure 9 shows the integrated system's FRF response for several values of c1, it can be notified that by reducing the inner radius from 10mm to 1 mm, the first resonance amplitude of the response is decreased by 8 dB (24% reduction achieved) with shifting resonance frequency by 2 Hz. This result is acknowledged by another study, through examining the ways for obtaining maximum modulus ratio, which is due to shrinkage in longitudinal strain, and increasing F2MC tubes axial strain. It increases the moments in the tubes bonding locations with the cantilever beam as in Eq. (1, 2 and 82). In addition to more fluid entrance to the F2MC tubes and higher internal pressures (Eq. 61), [24]. But further reducing inner radius (c1) to 0.5 mm, the tube's internal cavity was restricted so much, blocked the fluid flow into the tubes due to a low generation of pressure difference, so, the tube's ability to dissipate energy was lost. Because the tube walls have high authority to volume change [25], the resulted first resonance amplitude of the response was 4 dB higher, but the second amplitude reduced clearly with an overall gain reduction by 5Hz.

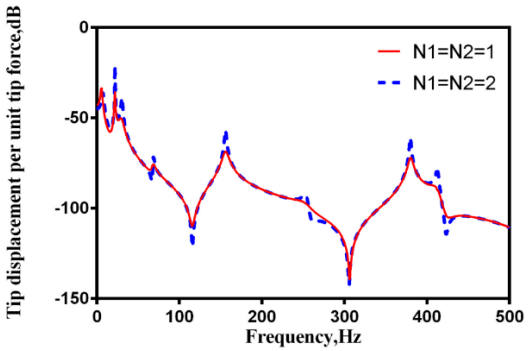

Fig. 8 FRF response of the system of two patches integrated above the beam, with different number of tubes: solid line for single tubes were used, and dashed for a pair of tubes used in both patches.

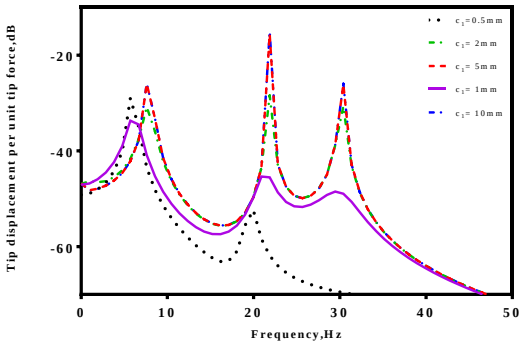

Fig. 9 FRF response of two patches of F²MC tubes integrated on the cantilever beam, with different tube sizes: inner radius c_1 = 0.5mm(dotted), 1mm (solid),2mm(dash-dotted), 5mm(dashed), and 10mm(dash-double dotted), the other radii c_2, c_3, and c_4 are selected as $1.7c_1$,$1.8c_1$, and $2.105c_1$ respectively.

Conclusion

In spite of most recent studies dealing with vibration control of cantilever structures focused active or semi-active vibration control, this study shaded a new light on damping treatment of cantilever beams by using passive vibration control. It analyzed a new approach for using F²MC tubes by integrating them as two separate patches above or under cantilever beams. It presented a simple way for mathematical modelling multi patches integrated on cantilever beam in different locations. A model of pair of F²MC tubes was modified to study two patches of single F²MC tube with their exactly half of length of single patch. Increasing the number of F²MC patches for controlling vibrations gives more desirable results than connecting several F²MC tubes inside one patch. The present study took benefit from selected layer thickness ratio for examining the sizes of F²MC tubes. Choosing the patch's joining points depends on the parameters that requested for controlling. For managing resonance frequency, it is better to bond the patches above and under the cantilever structures, but for reducing amplitude of vibrations, integrating the patches on the beam is the best choice.

Conflicts of Interest

The author declares that they have no conflicts of interest.

References

[1] R. Sharma, Hatraj, H. Pal, and S. R. Dutta, "Vibration Control of Cantilever Beam Based on Eddy Current Damping," *Pelagia Research Library, Advances in Applied Science Research*, vol. 2, pp. 429-438, 2011.

[2] C. D. Johnson, "Design of Passive Damping Systems," *Special 50th Anniversary Design Issue,Transcations of ASME*, vol. 117, pp. 171-176, June,1995 1995.

[3] R. Rusovici, J. J. Dosch, and G. A. Lesieutre, "Design of a Single Crystal Pizoceramic Vibration Absorber," *Journal of Intelligent Materials Systems and Structures*, vol. 13, pp. 705-712, November 2002 2002.

[4] J. Oh, S. Poh, M. Ruzzene, and A. Baz, "Vibration Control of Beams Using Electro-Magnetic Compressional Damping Treatment," *Journal of Vibration and Acoustics*, vol. 122, pp. 235-243, June, 2000 2000.

[5] A. Loghmani, M. Danesh, M. K. Kwak, and M. Keshmiri, "Vibration suppression of a piezo-equipped cylindrical shell in a broad-band frequency domain," *Journal of Sound and Vibration*, vol. 411, pp. 260-277, 2017.

[6] M. Philen, S. Ying, C. E. Bakis, K. W. Wang, and C. D. Rahn "Variable Stiffness Adaptive Structures utilizing Hydraulically Pressurized Flexible Matrix Composites with Valve Control," presented at the

47th AIAA/ASME/ASCE/AHS/ASC Structures, Structural Dynamics, and Materials Conference Newport, Rhode Island, 2006.

[7] S. Ying, P. M. Philen, E. B. Charles, K. W. Wang, and D. R. Christopher, "Nonlinear-elastic finite axisymmetric deformation of flexible matrix composite membranes under internal pressure and axial force," *Composites Science and Technology,* vol. 66, pp. 3053-3063, 2006.

[8] Ying Shan, Michael Philen, A. Lotfi, S. Li, C. E. Bakis, C. D. Rahn, and K. W. Wang, "Variable Stiffness Structures Utilizing Fluidic Flexible Matrix Composites," *Journal of Intelligent Materials Systems and Structures,* vol. 20, pp. 443-456, 2009.

[9] A. Vashisth, B. Zhu, B. M. Wimmer, C. E. Bakis, and C. D. Rahn, "Evaluation of millimeter-size fluidic flexible matrix composite tubes," in *Proceedings of the ASME 2013 Conference on Smart Materials, Adaptive Structures and Intelligent Systems*, Snowbird,Utah,USA, 2013, p. 9.

[10]A. Lotfi-Gaskarimahalle, Lioyd H. Scarborough , Christopher D. Rahn, and Edward C. Smith, "Fluidic Composite Tuned Vibration Absorbers," in *Proceedings of the ASME 2009 Conference on Smart Materials, Adaptive Structures and Intelligent Systems*, Oxnard, California, USA, 2009, pp. 1-8.

[11]M. Philen, "Fluidic flexible matrix composite semi-active vibration isolation mounts," *Journal of Intelligent Material Systems and Structures,* vol. 23, pp. 353-363, 2011.

[12]B. Zhu, M. J. Krott, C. D. Rahn, and E. B. Charles, "Experimental characterization of a cantilever beam with a fluidic flexible matrix composite vibration tratment," in *Proceedings of the ASME 2014 International Design Engineering Technical Conferences &Computers and Information in Engineering* Buffalo, NewYork USA, 2014, p. 6.

[13]B. Zhu, C. D. Rahn, and C. E. Bakis, "Fluidic flexible matrix composite damping treatment for a cantilever beam," *Journal of Sound and Vibration,* vol. 340, pp. 80-94, 2015.

[14]M. J. Krott, K. Miura, S. LaBarge, D. R. Christopher, E. C. Smith, and P. Q. Romano, "Tube Compliance Effects on Fluidic Flexible Matrix Composite Devices for Rotorcraft Vibration Control," in *56th AIAA/ASCE/AHS/ASC Structures, Structural Dynamics, and Materials Conference*, Kissimmee, Florida., 2015, p. 12.

[15]K. Miura, M. Krott, E. Smith, C. Rahn, and P. Q. Romano, "Experimental Validation of Tailboom Vibration Control Using Fluidic Flexible Matrix Composite Tubes," presented at the AHS 71st Annual Forum of the American Helicopter Society, Virginia Beach, Virginia, 2015.

[16]J. M. Gere, *Mechanics of Materials*, 6th ed.: Thomson Brooks/Cole, 2004.

[17]S. G. Lekhnitskii, *Theory of Elasticity of an Anisotropic body*, 2nd ed. Moscow: Mir Publishers, 1977.

[18]C. T. Sun and S. Li, "Three-Dimensional Effective Elastic Constants for Thick Laminates," *Journal of Composite Materials,* vol. 22, pp. 629-639, July 1988 1988.

[19]H. Bakaiyan, H. Hosseini , and E. Ameri "Analysis of multi-layered filament-wound composite pipes under combined internal pressure and thermomechanical loading with thermal variations," *Composite Structures,* vol. 88, pp. 532-541 2009.

[20]A. P. Boresi, R. J. Schmidt, and O. M. Sidebottom, *Advanced Mechanics of materials*, 5th ed. USA: John Willey & Sons Inc, 1993.

[21]Junda Chen, Guangtao Lu, Yourong Li, Tao Wang, Wenxi Wang, and G. Song, "Experimental Study on Robustness of an Eddy Current-Tuned Mass Damper," *Applied Science-BASEL,* vol. 7, 2017.

[22]B. Zhu, C. D. Rahn, and C. E. Bakis, "Fluidic flexible matrix composite vibration absorber for a cantilever beam," *Journal of Vibration and Acoustics,* vol. 137, p. 11, 2014.

[23]L. Hongnan, Z. Peng, S. Gangbing, P. Devendra, and M. Yilung, "Robustness study of the pounding tuned mass damper for vibration control of subsea jumpers," *Smart Materials and Structures,* vol. 24, p. 095001, 2015.

[24]Y. Chen, J. Sun, Y. Liu, and J. Leng, "Experiment and analysis of fluidic flexible matrix composite (F^2MC) tube," *Journal of Intelligent Material Systems and Structures,* 2012.

[25]Z. Zhang, M. Philen, and W. Neu, "A biologically inspired artificial fish using flexible matrix composite actuators: Analysis and experiment," *Smart Materials and Structures,* vol. 19, pp. 1-11, 2010.

نموذج جديد للتحكم في الاهتزاز السلبي لعمود مثبت من طرف واحد باستخدام صفين من أنابيب مرنة متكونة من مواد مركبة ومليئة بالسوائل

شيرين عثمان محمد **نزاد احمد حسين**

ميكانيك وميكانيكا الكترونية، كلية الهندسة، جامعة صلاح الدين، اربيل– العراق

shireen.muhammad@su.edu.krd nazhad.hussein@su.edu.krd

الخلاصة

يعتبر الانبوب المرن المتكون من عده مواد مركبة بشكل مصفوفه متناسقة من التقنيات الناشئة والحديثة اللتي تتميز بخفه وزنها وقدرتها الفائقة في امتصاص الاهتزازات والتحكم بها. يقدم هذا البحث نموذجا جديدا لحل مشكلة الاهتزازات الناتجة عن جسم مثبت من جهة واحده ومثبته عليه الانابيب المرنة. تم اشتقاق نموذج رياضي وباستخدام المعادلات اللازمة لمعرفه مدى تاثير هذه الانابيب على الجسم. تم اشتقاق هذه المعادلات بالاعتماد على نظريات اولير وبيرنولي للمرونه. بحثت هذه الدراسة أداء النموذج الجديد للتثبيط مع تباين في حجم الأنبوب؛ وضع الترابط للانابيب على الحزمة في حالتين مختلفتين: الحالة الاولى تمت دراسة النموذج عند تغيير المسافه بينهما، وفي الحاله الثانية تم تثبيت أحدهما في اعلى النموذج والاخر اسفله. توضح النتائج التحليلية العلاقه بين الضبط الصحيح لحجم الانابيب نسبه الى نصف قطر الطبقة الداخلية، ونقاط التكامل هي المعلمات الأساسية للتحكم في الاهتزاز السلبي والتي تحقق تخفيض في مدى الاستجابه في وضع التقوس العمودي الرئيسي بشكل فعال.

الكلمات الدالة: وحدة تحكم الاهتزاز السلبي، أنابيب مرنة متكونة من مواد مركبة ومليئة بالسوائل، النموذج الرياضي، التخميد، دالة استجابة التردد.